Research Article | Vol. 28, No. 21 / 12 October 2020 / Optics Express 31076
Optics EXPRESS

Efficient generation of heralded narrowband color-entangled states

XIAO-JUN ZHANG,[1] JIN-HUI WU,[1,6] G. C. LA ROCCA,[2,7] AND M. ARTONI[3,4,5,8]

[1]School of Physics, Northeast Normal University, Changchun 130024, China
[2]Scuola Normale Superiore and CNISM, Pisa, Italy
[3]European Laboratory for Non-Linear Spectroscopy, Sesto Fiorentino, Italy
[4]Department of Engineering and Information Technology, University of Brescia, Italy
[5]Istituto Nazionale di Ottica (INO-CNR), Italy
[6]jhwu@nenu.edu.cn
[7]giuseppe.larocca@sns.it
[8]artoni@lens.unifi.it

Abstract: We show that narrowband two-color entangled single Stokes photons can be generated in a ultra-cold atoms sample via selective excitation of two spontaneous four-wave mixing (SFWM) processes. Under certain circumstances, the generation, heralded by the respective common anti-Stokes photon, is robust against losses and phase-mismatching and is remarkably efficient owing to balanced resonant enhancement of the two four-wave mixing processes in a regime of combined induced transparency. Maximally color-entangled states can be easily attained by adjusting the detunings of the external couplings and driving fields, even when these are quite weak.

1. Introduction

Over the past decade, much attention has been devoted to developing sources of non-classical light, such as single-photon and entangled-photon states. Combining techniques of linear and nonlinear optical processing, measurement postselection techniques and optical (homodyne) tomography has led to a number of pioneering experiments in which several non-classical optical states have been prepared and measured [1]. Entangled states is just an ubiquitous example and one that represents a cornerstone of most protocols [2] for foundations of quantum physics and for applications of quantum technologies, such as *e.g.* quantum information processing [3], quantum computers [4,5] and algorithms [6], quantum metrology [7] and other essential resources for next generation photonic quantum technologies [8,9].

It has also been known since the very beginning of quantum optics that nonclassical properties of optical states such as *e.g.* entanglement rely indeed on rather *weak-nonlinearities* and are furthermore vulnerable to *losses* [10–13] The quantum features of an optical state propagating through a lossy medium are shared with the environment and hence are lost when the environment is traced over. Therefore it has been a long standing goal to minimize the amount of losses while maximizing the strength of the nonlinearities in the preparation of these states in order to make them useful for quantum networks [14], quantum memories [15], quantum key distribution [16,17] and more generally for quantum information processing [3].

Approaches based on nonlinear optical effects such as spontaneous parametric down-conversion and spontaneous four-wave mixing have been widely employed for decades to generate entangled photon pairs. Entangled photons, generated by spontaneous parametric down-conversion (SPDC) in nonlinear crystals [18–23], are endowed with *large bandwidths*, typically on the order of several THz, which makes them unfortunately unfit for quantum memory devices or repeaters based on atomic interfaces [24–28]. Spontaneous four-wave mixing (SFWM) is better suited to

#401551 https://doi.org/10.1364/OE.401551
Journal © 2020 Received 6 Jul 2020; revised 24 Aug 2020; accepted 1 Sep 2020; published 2 Oct 2020

Optics EXPRESS

the task of generating narrowband photons [28–30] as witnessed by the recent development in the generation of bi-photons in atomic vapors [31,32]. In this case configurations comprising two [33,34], three [35] or four atomic levels [36,37] suitably driven by external (classical) fields have been thoroughly investigated.

Up to now, several SFWM based schemes to generate *pairs* of polarization entangled [38], position-momentum entangled [39] and hyperentangled photons [40] sources have been proposed and experimentally demonstrated. More recently, frequency-entanglement has also been proposed in the context of a two-color entangled *single-photon* [41,42], where two frequency (color) modes become entangled through sharing of a single photon, very much alike spatial entanglement where the single-photon shares instead two distinct paths.

Intrinsic to this scheme is the three-level atomic configuration, which prevents from balancing the resonant enhancement [43–45] of the nonlinearities associated with the two SFWM processes responsible for entanglement. This appears to limit the efficiency of the entanglement generation.

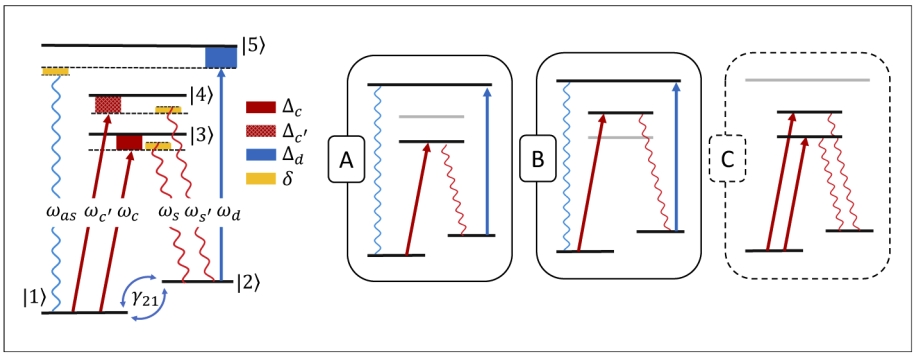

Fig. 1. *Single-photon Color-entanglement Generation.* Three sufficiently *weak* laser beams (ω_c, $\omega_{c'}$, ω_d) may promote the spontaneous generation of two distinct pairs of Stokes and anti-Stokes photons. This occurs through third-order nonlinear spontaneous processes where the driving (ω_d) and coupling (ω_c) fields yield the Stokes and anti-Stokes pair $\{\omega_s, \omega_{as}\}$ whereas the same driving (ω_d) and the other coupling (ω_c') yields the second pair $\{\omega_s', \omega_{as}\}$. The two distinct processes are displayed separately in panels (A) and (B). The two couplings alone (ω_c, ω_c') are instead responsible for the energy exchange between the two Stokes photons ω_s and $\omega_{s'}$ as depicted in panel (C). The atomic level scheme comprises the three excited states $|3\rangle = |5\,^2P_{1/2}, F = 1, m_F = 0\rangle$, $|4\rangle = |5\,^2P_{1/2}, F = 2, m_F = 0\rangle$ and $|5\rangle = |5\,^2P_{3/2}, F = 2, m_F = 0\rangle$ and the two close ground–hyperfine states $|1\rangle = |5\,^2S_{1/2}, F = 1, m_F = -1\rangle$ and $|2\rangle = |5\,^2S_{1/2}, F = 1, m_F = 1\rangle$. This choice of states, where all optical transitions have approximately the same dipole matrix elements $|\mu| \approx 0.73 \times 10^{-29}$ C·m and coherence decay rate γ and with all processes (A-B-C) further sharing the common spin coherence γ_{12} (*see* Sect. 3), makes the level configuration symmetric. This holds, in particular, for the two non-linear mixing processes in panels (A) and (B), the two key four-wave mixing processes (that may be interpreted as the two indistinguishable paths in the double-slit experiment) responsible for the entanglement generation, whereas panel (C) describes an additional process that can be suppressed (*see text*). We can control the efficiency of the generation process through the detuning Δ_c, $\Delta_{c'}$, Δ_d and the Rabi frequency Ω_c, $\Omega_{c'}$ and Ω_d of the applied beams as well as through the two-photon detuning δ. A magnetic field removes all degeneracies with respect to the sub-levels $\{m_F\}$ and selectivity is ensured by polarization selection rules: the laser field ω_c that drives the transition $|1\rangle \leftrightarrow |3\rangle$ is assumed to be σ^+- polarized, yet without coupling the atoms through the $|2\rangle \leftrightarrow |3\rangle$ transition, though the two ground states $|1\rangle$ and $|2\rangle$ lie close to each other. For the same reason, $\omega_{c'}$ and ω_d are assumed to be σ^+- and σ^-- polarized, respectively.

Optics EXPRESS

In this paper, we propose an efficient novel approach to the single-photon color-entanglement generation problem. The efficiency of the generation process hinges on the balanced resonant enhancement of two specific SFWM processes responsible for the entanglement. This is harnessed through a five atomic-level configuration driven by "two" couplings and "one" driving field where each coupling and driving *pair* is two-photon resonant with the respective Stokes and (common) anti-Stoke modes (See Fig. 1). Despite the apparent complexity of the multi-levels configuration, the present proposal scores a remarkable increase in the *generation efficiency* when compared to apparently simpler schemes [41]. This mainly hinges on the concomitant resonant enhancement of the relevant third-order susceptibilities in a regime of induced transparency which warrants for a generation process that is robust against loss and phase-mismatching. Both are crucial for quantum applications and processing [3]. Control of the efficiency is moreover rather straightforward and attained by adjusting the external fields parameters (See Fig. 1). Bright narrowband maximally color-entangled states can be attained *e.g.* with very weak and resonant coupling and driving fields.

We give in Sect. 2–3 the linear and third-order susceptibilities along with the archetype of an atomic interface in Sec. 3 needed to describe the entanglement generation in Sec. 4. Details on the derivation of the susceptibilities are provided in the Appendix. Some properties of the color-entangled single-photon state are presented therein along with an analysis of the main factors affecting the generation process efficiency. In addition, specific generation results are discussed in the subsections 4.1 and 4.2 respectively for a large detuning driving and a resonant driving regime. We present instead in the following Sect. 5 a scheme to engineer both efficiency and degree of entanglement while the conclusions are summarized in Sec. 6.

2. Model susceptibilities

The generation scheme follows from a four-photons spontaneous four-wave mixing process [38] in a multi-level third-order nonlinear medium where, in the presence of a weak *classical* coupling ω_c ($\omega_{c'}$) and a driving ω_d beam, Stokes and anti-Stokes photon pairs emerge. Two of such processes, one leading to the emission of a *Stokes* (ω_s) and an *anti-Stokes* (ω_{as}) photon–pair and the other leading to the emission of the same *anti-Stokes* (ω_{as}) yet a different *Stokes* (ω_s') photon are separately sketched in Figs. 1(A) and (B). The nonlinear mixing process leading *e.g.* to the generation of the first pair $\{\omega_{as}, \omega_s\}$ hinges on the formation of a *common* collective atomic spin excitation between levels $|1\rangle$ and $|2\rangle$ via the coupling and the driving that are responsible for the cycling transitions between the two lower levels through the upper levels $|3\rangle$ and $|5\rangle$. Similarly for the second pair $\{\omega_{as}, \omega_s'\}$, which involves the upper levels $|4\rangle$ and $|5\rangle$.

Control over the generation process occurs through the coupling and driving fields. We denote *e.g.* by $\Delta_c = \omega_{31} - \omega_c$ the coupling's detuning from the resonant frequency of the transition $|1\rangle \leftrightarrow |3\rangle$ and with $\Omega_c = \mu_{13}E_c/2\hbar$ its Rabi frequency, where E_c stands for the field's amplitude and μ_{13} for the dipole matrix element of the same transition. The other detunings $\Delta_{c'}$ and Δ_d and Rabi frequencies $\Omega_{c'}$ and Ω_d are defined in the same manner. We further denote by $\hat{E}_m^+$, with $m \in \{s, s', as\}$, the field operator for the Stokes or anti-Stokes photon

$$\hat{E}_m^+(\mathbf{r}, t) = \frac{1}{\sqrt{\pi}} \int d\omega \sqrt{\frac{2\hbar\omega}{c\epsilon_0 A}} e^{i[\mathbf{k}_m(\omega)\cdot\mathbf{r} - \omega t]} \hat{a}_m. \tag{1}$$

The Stokes photon's frequency ω_s detuning from the corresponding transition is $\Delta_s = \omega_{32} - \omega_s$ with the other detunings $\Delta_{s'}$ and Δ_{as} defined in the same manner. In addition, we introduce the two-photon detuning

$$\Delta_c - \Delta_s = \Delta_{c'} - \Delta_{s'} = -(\Delta_d - \Delta_{as}) = \delta \tag{2}$$

which we assume to be the same for each conjugate pair of classical-photon fields.

Optics EXPRESS

We can thus work in the rotating frame approximation with a time independent Hamiltonian $\hat{H}$. The atomic dynamics, in particular, can be described by the Heisenberg-Langevin equations of motion for populations ($\hat{\sigma}_{ii}$) and coherences ($\hat{\sigma}_{ij}$),

$$i\hbar\frac{\partial}{\partial t}\hat{\sigma}_{ij} = [\hat{\sigma}_{ij}, \hat{H}] = [\hat{\sigma}_{ij}, \hat{H}_0 + \hat{H}_I], \tag{3}$$

where as usual $\hat{H}_0$ and $\hat{H}_I$ denote the (free) atoms and the electric dipole interaction parts [46]. As the Stokes and anti-Stokes fields represent single-photons, they are taken to be much weaker than the two applied couplings and driving, which warrant for a perturbative approach by replacing $\hat{E}^{\pm}_m \rightarrow \epsilon\hat{E}^{\pm}_m$, where ϵ is a small parameter. This enables us to expand populations and coherences in powers of ϵ,

$$\hat{\sigma}_{ij} = \hat{\sigma}^{(0)}_{ij} + \epsilon\hat{\sigma}^{(1)}_{ij} + \epsilon^2\hat{\sigma}^{(1)}_{ij}\cdots \tag{4}$$

leading to sets of zero-order and first-order evolution equations namely for $\hat{\sigma}^{(0)}_{ij}$ and for $\hat{\sigma}^{(1)}_{ij}$. The former describes the free evolution in the presence of the applied coupling and driving beams while the latter describes the evolution when weak nonlinear Stokes and anti-Stokes fields are being generated. One can obtain the solution for $\hat{\sigma}^{(0)}_{ij}$ as shown in the Appendix Eqs. (24a)–(25j). Provided all detunings are sufficiently larger than the excited states decay rate (optical transitions), *i.e.* $\Delta_n \gg \Gamma_{j'j}$, or all classical beams Rabi frequencies are sufficiently small when $\Delta_n \rightarrow 0$, *i.e.* $\Omega_n \ll \Gamma_{j'j}$, with $n \in \{c, c', d\}$, $j' \in \{3, 4, 5\}$, $j \in \{1, 2\}$, then the zero-order solutions for the excited states populations are vanishing,

$$\sigma^{(0)}_{jj} \rightarrow 0, \quad j \in \{3, 4, 5\}. \tag{5}$$

We checked that for the parameters we used in Sect. 4.1 (large detuning case) and in Sect. 4.2 (resonant case), the excited states (overall) zeroth-order population $\sigma^{(0)}_{jj}, j \in \{3, 4, 5\}$ obtained from solving (A2a-A2j) does not exceed 5‰. For the single-photon generation process to be reliable negligible excited states populations are indeed required. While the solutions for the ground populations satisfy the relation

$$\frac{\sigma^{(0)}_{11}}{\sigma^{(0)}_{22}} = \frac{|\Omega_d|^2}{(|\Omega_c|^2 + |\Omega_{c'}|^2)} \tag{6}$$

We can now use (5–6) to obtain steady-state expressions for the first-order optical coherences which are then used to attain the macroscopic polarization exhibited by the *anti-Stokes* photon (ω_{as})

$$\begin{aligned}\hat{p}_{15} &= \epsilon_0\chi_{as}\hat{E}^{+}_{as} \\ &\quad + \epsilon_0\chi^{(3)}_{as,s}E_cE_d\hat{E}^{-}_{s} + \epsilon_0\chi^{(3)}_{as,s'}E_{c'}E_d\hat{E}^{-}_{s'}.\end{aligned} \tag{7a}$$

and that exhibited by the (two) *Stokes* photons ($\omega_{s,s'}$) i.e.

$$\begin{aligned}\hat{p}_{23} &= \epsilon_0\chi_{s}\hat{E}^{+}_{s} \\ &\quad + \epsilon_0\chi^{(3)}_{s,as}E_cE_d\hat{E}^{-}_{as} + \epsilon_0\chi^{(3)}_{s,s'}E_cE^{*}_{c'}\hat{E}^{+}_{s'},\end{aligned} \tag{7b}$$

$$\begin{aligned}\hat{p}_{24} &= \epsilon_0\chi_{s'}\hat{E}^{+}_{s'} \\ &\quad + \epsilon_0\chi^{(3)}_{s',as}E_{c'}E_d\hat{E}^{-}_{as} + \epsilon_0\chi^{(3)}_{s',s}E^{*}_{c}E_{c'}\hat{E}^{+}_{s}.\end{aligned} \tag{7c}$$

Here

$$\chi_{as} = i\mathcal{N}\sigma^{(0)}_{11}\frac{|\mu_{15}|^2}{\epsilon_0\hbar}\frac{g_{12}g_{32}g_{35}g_{42}g_{45}}{\mathcal{D}^6}, \tag{8a}$$

Optics EXPRESS

$$\chi_s = i\mathcal{N}\sigma_{22}^{(0)}\frac{|\mu_{23}|^2}{\epsilon_0\hbar}\frac{g_{21}g_{24}g_{51}g_{53}g_{54}}{(\mathcal{D}^*)^6}, \tag{8b}$$

$$\chi_{s'} = i\mathcal{N}\sigma_{22}^{(0)}\frac{|\mu_{24}|^2}{\epsilon_0\hbar}\frac{g_{21}g_{23}g_{51}g_{53}g_{54}}{(\mathcal{D}^*)^6}, \tag{8c}$$

denote the *linear* susceptibilities, while

$$\chi_{as,s}^{(3)} = -i\mathcal{N}\frac{\mu_{13}\mu_{15}\mu_{23}\mu_{25}}{4\epsilon_0\hbar^3}\frac{g_{42}g_{45}}{\mathcal{D}^6}\left[\frac{g_{32}g_{35}}{g_{13}}\sigma_{11}^{(0)} + \left(g_{12}+g_{35}+\frac{g_{12}g_{32}}{g_{25}}\right)\sigma_{22}^{(0)}\right], \tag{9a}$$

$$\chi_{as,s'}^{(3)} = -i\mathcal{N}\frac{\mu_{15}\mu_{14}\mu_{25}\mu_{24}}{4\epsilon_0\hbar^3}\frac{g_{32}g_{35}}{\mathcal{D}^6}\left[\frac{g_{42}g_{45}}{g_{14}}\sigma_{11}^{(0)} + \left(g_{12}+g_{45}+\frac{g_{12}g_{42}}{g_{25}}\right)\sigma_{22}^{(0)}\right], \tag{9b}$$

$$\chi_{s,as}^{(3)} = -i\mathcal{N}\frac{\mu_{13}\mu_{15}\mu_{23}\mu_{25}}{4\epsilon_0\hbar^3}\frac{g_{24}g_{54}}{(\mathcal{D}^*)^6}\left[\left(g_{21}+g_{53}+\frac{g_{21}g_{51}}{g_{13}}\right)\sigma_{11}^{(0)} + \frac{g_{51}g_{53}}{g_{25}}\sigma_{22}^{(0)}\right], \tag{9c}$$

$$\chi_{s',as}^{(3)} = -i\mathcal{N}\frac{\mu_{15}\mu_{14}\mu_{25}\mu_{24}}{4\epsilon_0\hbar^3}\frac{g_{23}g_{53}}{(\mathcal{D}^*)^6}\left[\left(g_{21}+g_{54}+\frac{g_{21}g_{51}}{g_{14}}\right)\sigma_{11}^{(0)} + \frac{g_{51}g_{54}}{g_{25}}\sigma_{22}^{(0)}\right], \tag{9d}$$

$$\chi_{s,s'}^{(3)} = -i\mathcal{N}\frac{\mu_{13}\mu_{23}\mu_{41}\mu_{42}}{4\epsilon_0\hbar^3}\frac{g_{51}g_{53}g_{54}}{(\mathcal{D}^*)^6}\left[\left(\frac{g_{24}}{g_{41}}+\frac{g_{21}g_{24}}{g_{13}g_{43}}+\frac{g_{21}g_{24}}{g_{41}g_{43}}\right)\sigma_{11}^{(0)} + \sigma_{22}^{(0)}\right], \tag{9e}$$

$$\chi_{s',s}^{(3)} = -i\mathcal{N}\frac{\mu_{14}\mu_{24}\mu_{31}\mu_{32}}{4\epsilon_0\hbar^3}\frac{g_{51}g_{53}g_{54}}{(\mathcal{D}^*)^6}\left[\left(\frac{g_{23}}{g_{31}}-\frac{g_{21}g_{23}}{g_{14}g_{34}}-\frac{g_{21}g_{23}}{g_{31}g_{34}}\right)\sigma_{11}^{(0)} + \sigma_{22}^{(0)}\right], \tag{9f}$$

denote the *nonlinear* (third-order) susceptibilities, with

$$\mathcal{D}^6 = g_{12}g_{15}g_{32}g_{35}g_{42}g_{45} \times \left(1+\frac{|\Omega_c|^2}{g_{12}g_{32}}+\frac{|\Omega_{c'}|^2}{g_{12}g_{42}}+\frac{|\Omega_d|^2}{g_{12}g_{15}}\right).$$

and with g_{ij} the *complex decay* functions whose imaginary and real parts denote respectively the detuning and coherence decay rate γ_{ij} associated with the corresponding transition, namely $g_{13} = \gamma_{13} + i\Delta_c$, $g_{14} = \gamma_{14} + i\Delta_{c'}$, $g_{12} = \gamma_{12} + i\delta$, $g_{13} = \gamma_{13} + i\Delta_c$, $g_{14} = \gamma_{14} + i\Delta_{c'}$, $g_{15} = \gamma_{15} + i\Delta_{\rm as}$, $g_{23} = \gamma_{23} - i(\delta - \Delta_c)$, $g_{24} = \gamma_{24} - i(\delta - \Delta_{c'})$, $g_{25} = \gamma_{25} - i(\delta - \Delta_{\rm as})$, $g_{34} = \gamma_{34} - i(\Delta_c - \Delta_{c'})$, $g_{35} = \gamma_{35} - i(\Delta_c - \Delta_{\rm as})$, $g_{45} = \gamma_{45} - i(\Delta_{c'} - \Delta_{\rm as})$, and $g_{ij} = g_{ji}^*$.

The susceptibility χ_{as} in (7a), *e.g.*, represents the linear contribution to the medium polarization [47] at the anti-Stokes frequency ω_{as} and its real and imaginary parts are known to describe respectively the medium dispersion and absorption of photons at the anti-Stokes frequency ω_{as} [48]. Similarly for the linear Stokes susceptibilities $\chi_{s,s'}$ in (7b–7c). The spontaneous nonlinear (four) wave-mixing of a coupling (ω_c), driving (ω_d), anti-Stokes (ω_{as}) and Stokes (ω_s) photon

Optics EXPRESS

contributes to the medium non-linear polarization at ω_{as} and at ω_s respectively through the susceptibility $\chi^{(3)}_{as,s}$ in (7a) and $\chi^{(3)}_{s,as}$ in (7b). Both processes are sketched in Panel A of Fig. 1. The two processes can also be interpreted as arising from the cycling transition $|1\rangle \rightarrow |3\rangle \rightarrow |2\rangle \rightarrow |5\rangle$ leading to the emission of a photon at frequency ω_{as}, yielding a nonlinear polarization $\propto \chi^{(3)}_{as,s}$ at the $|5\rangle \leftrightarrow |1\rangle$ transition or arising from the transition $|2\rangle \rightarrow |5\rangle \rightarrow |1\rangle \rightarrow |3\rangle$ leading to the emission of a photon at frequency ω_s and yielding a nonlinear polarization $\propto \chi^{(3)}_{s,as}$ at the $|3\rangle \leftrightarrow |2\rangle$ transition. The other nonlinear contributions to the polarization(s) can be discussed in much the same way namely those proportional to $\chi^{(3)}_{as,s'}$ and $\chi^{(3)}_{s',as}$, which we sketch in Panel B of Fig. 1, and the nonlinear contributions proportional to $\chi_{s',s}$ and $\chi_{s,s'}$, sketched in Panel C of Fig. 1.

3. Atomic interface model

The interface setup we examine here to discuss the entanglement generation efficiency adopts atomic transitions appropriate to a cold ^{87}Rb sample (Fig. 1). The level scheme involves both D_1 and D_2 transitions with the three *excited* states $|3\rangle = |5\,^2P_{1/2}, F = 1, m_F = 0\rangle$, $|4\rangle = |5\,^2P_{1/2}, F = 2, m_F = 0\rangle$ and $|5\rangle = |5\,^2P_{3/2}, F = 2, m_F = 0\rangle$ and the two close *ground–hyperfine* states $|1\rangle = |5\,^2S_{1/2}, F = 1, m_F = -1\rangle$ and $|2\rangle = |5\,^2S_{1/2}, F = 1, m_F = 1\rangle$.

For such a level configuration the *population decay* rates from the three excited states and the *coherence decay* rates of the excited *to* ground states and of the excited *to* excited states are approximately equal. We take $\Gamma_{j'j} = \Gamma = 3$ MHz, with $j \in \{1, 2\}$ and $j' \in \{3, 4, 5\}$ for the single-channel excited state decay. Because $\gamma_{ij} = \frac{1}{2}\sum_k \Gamma_{ik} + \frac{1}{2}\sum_{k'} \Gamma_{jk'}$ is half the sum of the overall decay rates from levels $|i\rangle$ and $|j\rangle$, when taking a common single-channel excited state decay $\Gamma_{j'j} = \Gamma$, with $j \in \{1, 2\}$ and $j' \in \{3, 4, 5\}$, optical transitions will share the common dephasing $\gamma_{51} \simeq \gamma_{52} \simeq \gamma_{41} \simeq \gamma_{42} \simeq \gamma_{31} \simeq \gamma_{32} = \gamma_{eg} \simeq \Gamma$, yet with the other coherences decaying at $\gamma_{54} \simeq \gamma_{53} \simeq \gamma_{43} \simeq \gamma_{ee'} = 2\Gamma$. The two close ground levels (*spin*) coherence is here taken to decay with $\gamma_{12} \simeq 5 \times 10^{-4}\,\Gamma$ [49].

For the atomic levels of Fig. 1, $|\mu_{13}| = |\mu_{14}| = |\mu_{23}| = |\mu_{24}| = \sqrt{1/12} \times 2.5377 \times 10^{-29}$ Cm $= 0.7326 \times 10^{-29}$ Cm while $|\mu_{15}| = |\mu_{25}| = \sqrt{1/24} \times 3.58424 \times 10^{-29}$ Cm $= 0.7316 \times 10^{-29}$ Cm. All the optical transitions have then approximatly the same dipole moment $\mu \simeq 0.73 \times 10^{-29}$ Cm (see e.g. [50]).

Then, to a very good approximation,

$$|\mu_{jj'}| \approx |\mu|, \text{with } j \in \{1, 2\}, j' \in \{3, 4, 5\}. \tag{10}$$

This makes the two non-linear processes (A) and (B) in Fig. 1 symmetric. This amounts to say, in turn, that generation of the two Stokes photons via spontaneous scattering through the two distinct excited states $|3\rangle$ and $|4\rangle$ occurs much in the same way so as to render the two four-wave mixing processes (A) and (B) *indistinguishable*.

We further anticipate some important properties of the susceptibilities that are to be used in the next section. When (10) holds along with

$$\Delta_c = \Delta_{c'} \tag{11}$$

it can be shown in fact that $\chi^{(3)}_{as,s} = \chi^{(3)}_{as,s'}$, and $\chi^{(3)}_{s,as} = \chi^{(3)}_{s',as}$. The above condition (11) means that the (two) couplings frequency difference matches exactly the energy separation between level $|3\rangle$ and $|4\rangle$ or equivalently that the emitted Stokes photons are equally detuned from the relevant transitions. Through the condition (11) we can further reduce the number of complex decay functions, *i.e.*, $g_{54} \simeq g_{53}, g_{42} \simeq g_{32}$ and $g_{41} \simeq g_{31}$.

It is also worth noting that the five-level configuration of Fig. 1, which will be used in the following Sec. 4(A-B) to assess the generation efficiency in a cold ^{87}Rb sample, may well fit other atomic gas species such as Cesium atoms [51,52] as well as solid media such as quantum dots in semiconductors [53] or nitrogen-vacancy centers in diamond [54].

Optics EXPRESS

4. Generation of the entangled states

In the interaction picture, the effective Hamiltonian describing the photon-atom interaction can be written as [55,56]

$$\hat{H}_I = \frac{\epsilon_0 A}{4}\int_{-\frac{L}{2}}^{\frac{L}{2}} dz\Big(\chi_A^{(3)}E_cE_d\hat{E}_{as}^-\hat{E}_s^- + \chi_B^{(3)}E_{c'}E_d\hat{E}_{as}^-\hat{E}_{s'}^- + \chi_{s,s'}^{(3)}E_{c'}^*E_cE_s^-E_{s'}^+ + \chi_{s',s}^{(3)}E_{c'}E_c^*E_{s'}^-E_s^+\Big) + \text{H.c.} \tag{12}$$

where we denote by $\chi_A^{(3)} = \chi_{as,s}^{(3)} + \chi_{s,as}^{(3)}$ and by $\chi_B^{(3)} = \chi_{as,s'}^{(3)} + \chi_{s',as}^{(3)}$. Here we assume that the Stokes and anti-Stokes photons are collected within a very small angle with respected to z direction along which the coupling and the driving fields travel together. The first term in (12), proportional to $\chi_A^{(3)}$, relates to the mixing process in Panel A of Fig. 1 and is responsible for the generation of the Stokes and anti-Stokes pair $\{\omega_s, \omega_{as}\}$ from one of the two couplings and the driving field. The second term, proportional to $\chi_B^{(3)}$, is responsible for the generation of a different photon pair $\{\omega_s', \omega_{as}\}$ through a similar process as depicted in Panel B in Fig. 1. For weak nonlinear interactions (*weak spontaneous scattering limit)* [57], we may limit ourselves to two-photons excitations so that the resulting state can be described to the first-order perturbation theory in which higher-order terms in the expansions corresponding to more than two-photons excitations are neglected, see also [41,57]. Then we have

$$\begin{aligned}|\Psi\rangle_{\text{out}} &\simeq \left(\mathbf{1} - \frac{i}{\hbar}\int_{-\infty}^{\infty} dt\hat{H}_I\right)|0\rangle \\ &= |0\rangle + \int d\omega\Big[f_A(\omega_c+\omega_d-\omega,\omega)\hat{a}_{as}^\dagger(\omega_c+\omega_d-\omega)\hat{a}_s^\dagger(\omega) \\ &\qquad + f_B(\omega_{c'}+\omega_d-\omega,\omega)\hat{a}_{as}^\dagger(\omega_{c'}+\omega_d-\omega)\hat{a}_{s'}^\dagger(\omega)\Big]|0\rangle.\end{aligned} \tag{13}$$

The last two additional terms in (12), describing the conversion of the two Stokes photons $\omega_{s'}$ and ω_s into one another, are proportional to $\hat{E}_s^+$ and $\hat{E}_{s'}^+$ and do not contribute to $|\Psi\rangle_{\text{out}}$. We further may rewrite the two complex amplitudes

$$f_A(\omega,\omega') = -i\frac{\sqrt{\omega\omega'}}{4\pi c}\chi_A^{(3)}(\omega,\omega')E_cE_d\,\delta_A^{(L)}L \tag{14}$$

$$f_B(\omega,\omega') = -i\frac{\sqrt{\omega\omega'}}{4\pi c}\chi_B^{(3)}(\omega,\omega')E_{c'}E_d\,\delta_B^{(L)}L \tag{15}$$

in terms of the (complex) mismatch function

$$\delta_A^{(L)} = e^{-i(\frac{\Delta k_A L}{2})}\text{sinc}(\frac{\Delta k_A L}{2}) \tag{16}$$

resulting from the spatial integral over the medium length L in (12). The overall (complex) wavevector mismatch Δk_A, which includes attenuation and the characteristic wave-vector mismatch among all fields involved in the process A, is computed from the index of refraction as, $\Delta k_A = \frac{\omega'}{c}n_{51}(\omega') + \frac{\omega}{c}n_{32}(\omega) - \frac{\omega_c}{c}n_{31}(\omega_c) - \frac{\omega_d}{c}n_{52}(\omega_d)$, where $n_{j'j}$ with $j' \in \{3,4,5\}$ and $j \in \{1,2\}$ is the *complex* refractive index experienced by the fields driving the respective transitions $|j'\rangle \leftrightarrow |j\rangle$, which in turn is computed from the usual (linear) susceptibility relation $n \sim 1 + \frac{1}{2}\chi$ [47]. Analogous expressions hold for Δk_B and $\delta_B^{(L)}$. Equation (13) anticipates a valuable feature of our proposal, namely, that the detection of an anti-Stokes photon (ω_{as}) projects

Optics EXPRESS

$|\Psi\rangle_{\rm out}$ into

$$|\Psi\rangle_p = [\langle 0_{as}|\hat{a}_{as}(\omega_{as})]|\Psi\rangle_{\rm out}. \tag{17}$$

i.e. state superposition of a (single) photon with frequency ω_s and $\omega_{s'}$. Substituting, in fact, (13) into (17) and with the help of $\left[\hat{a}_{as}(\omega), \hat{a}^{\dagger}_{as}(\omega')\right] = \delta(\omega - \omega')$ [58,59]

$$|\Psi\rangle_p = f_A(\omega_{as}, \omega_s)|1_s, 0_{s'}\rangle + f_B(\omega_{as}, \omega_{s'})|0_s, 1_{s'}\rangle \tag{18}$$

with $\omega_{s(s')} = \omega_{c(c')} + \omega_d - \omega_{as}$ set by the conservation of energy. In the state (18) f_A is the spectral amplitude component of the two-photon state probability distribution. Its magnitude square $|f_A|^2$ may then be considered as the spectral component of the generation rate of the pair $\{\omega_{as}, \omega_s\}$ for the process in Fig. 1(A). The overall probability of finding a single-Stokes photon at ω_s or $\omega_{s'}$,

$$\mathcal{P} = \left|\langle 1_s|\Psi\rangle_p\right|^2 + \left|\langle 1_{s'}|\Psi\rangle_p\right|^2 = |f_A|^2 + |f_B|^2, \tag{19}$$

may then be regarded as a figure of merit ($\mathcal{P}$) for the entanglement *generation efficiency*. Note that we assume that once an anti-Stokes photon is detected, an Stokes photon is detected for sure (100% heralding efficiency). Such genaration probability will essentially depend on three factors. *First*, it will depend on the mismatch functions $\delta^{(L)}_{A,B}$, *second*, on the Stokes photons absorption also affecting the mismatch above through $\Delta k_{A,B}$ and which we model here as $\mathcal{R}(\omega_{s,s'}) = 1 - \exp\left\{-\text{Im}[\chi_{s,s'}(\omega_{s,s'})]\omega_{s,s'}L/c\right\}$ and *third* on the nonlinear susceptibilities $\chi^{(3)}_{A,B}$. Clearly, large values of the mismatch functions and the non-linear susceptibilities ensure large frequency-conversions and hence increased efficiencies $\mathcal{P}$'s. Remarkably, all three factors can be optimized acting on the (common) detuning δ and to assess this important point we examine below the specific situation described in Sec. 2 following from (10–11) and for which we have $\chi_s = \chi_{s'}$ and $\chi^{(3)}_A = \chi^{(3)}_B$

4.1. Large detuning generation

We start discussing Stokes generation (ω_s) for the archetype setup discussed in Sect. 3 and the further assumption of large detunings and weak strengths of the two couplings and driving fields (See Fig. 1). The results shown in Fig. 2 would hold unchanged for the Stokes photon $\omega_{s'}$ because, under the above conditions, the two Stokes photons have the same absorption, phase mismatch, nonlinear susceptibility and hence generation efficiency. In particular, Fig. 2(a) shows that photon absorption is negligible at two-photon resonance $\delta = 0$ while maximum slightly below resonance (P_1); such a behaviour originates from the fact that when $\Delta \gg \Gamma$ the denominator of the linear susceptibilities can in general be written as

$$\mathcal{D}^6 \simeq 4\Delta^5(\delta - \Delta_{\rm eff} - i\gamma_{\rm eff}) \tag{20}$$

with

$$\Delta_{\rm eff} = -\frac{\Omega_c^2 + \Omega_{c'}^2 + \Omega_d^2}{\Delta}, \tag{21a}$$

$$\gamma_{\rm eff} = \frac{\Omega_c^2\gamma_{23} + \Omega_{c'}^2\gamma_{24} + \Omega_d^2\gamma_{15}}{\Delta^2}. \tag{21b}$$

The upper level is dynamically shifted [60] by the amount $\Delta_{\rm eff}$ while the generated/absorption Stokes line-width $\gamma_{\rm eff}$ being a suitable combination of the linewidths associated with the transitions in Panel A of Fig. 1. Just in correspondence of the absorption peak the absorption dependent mismatch $\delta^{(L)}_A$ in Fig. 2(b) exhibits a minimum bearing also a similar width, yet for the typical interface lengths $L \simeq 100$ μm we use here the mismatch function acquires values close to unity at two-photon resonance (P_1). Finally, the (dimensionless) nonlinear susceptibility in

Optics EXPRESS

Fig. 2(c) appears in this regime to be a pure imaginary function and vanishing when absorption is maximum. All three parameters combine together to yield the generation efficiency curve $\mathcal{P}$ plotted in Fig. 2(d) that has a maximum at P_3 where absorption less than that at the shifted value (P_2) and with a mismatch is closer to unity. Within this regime we can obtain a maximum efficiency $\mathcal{P}$ which is approximately 2×10^{-5}. By the way, the large-detuning case with $\Delta_c = \Delta_{c'} = \Delta_d$ unlike the present situation with $\Delta_c = \Delta_{c'} = -\Delta_d$ will make a significant increase in the coherence between excited levels $|3\rangle$ and $|5\rangle$ and between $|4\rangle$ and $|5\rangle$, causing amplification at the Stokes-photon transition (Im χ_m<0 $m \in \{s, s'\}$. The latter turns out to be detrimental for (Stokes) "single-photon" generation. As for the unbalancing of the detuning condition, We checked that $\Delta_c \neq \Delta_{c'}$ will quickly unbalance the two SFWM processes, even when equal coupling fields strengths are chosen, it hampers in the end the degree of the entanglement.

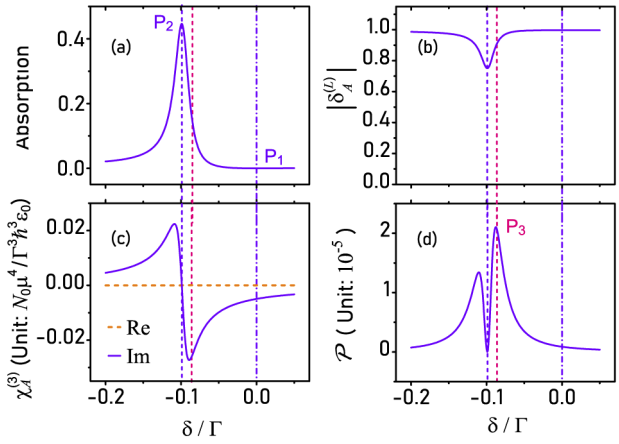

Fig. 2. *Large Detuning Color-Entanglement Generation.* (a) Absorption $\mathcal{R}$, (b) modulus of the mismatch function $\delta_A^{(L)}$, (c) real and imaginary part of the nonlinear susceptibility $\chi_A^{(3)}$ and (d) generation efficiency $\mathcal{P}$ as a function of the Stokes (ω_s) two-photon detuning δ (Panel A Fig. 1). Here $\Delta_c = \Delta_{c'} = 10\,\Gamma$, $\Delta_d = -10\,\Gamma$, $\Omega_c = \Omega_{c'} = 0.5\,\Gamma$, $\Omega_d = \sqrt{2}\Omega_c$. Plots in each panel are the same for Stokes photon $\omega_{s'}$ (Panel B Fig. 1). Characteristics points in the Stokes generation process are marked by vertical lines representing maximum generation efficiency (P_3), maximum (P_2) and minimum (P_1) absorption. Optimal efficiency occurs for Stokes photons at wavelengths $\lambda_s = 795.522$ nm, $\lambda_s' = 795.521$ nm, with equal detuning ($\delta = -0.08\Gamma$) from the relevant transitions, whereas the anti-Stokes photon is emitted at $\lambda_{as} = 780.778$ nm. The sample is $L = 100$ μm long and contains atoms with an average density of $N_0 = 5 \times 10^{11}$ cm^{-3} while other atomic parameters are as in Fig. 1.

4.2. Resonant generation

While keeping the above large-detuning regime as a reference case we now focus on a similar situation except that coupling and driving beams are now taken all resonant while having strengths one order of magnitude smaller. As before the discussion would hold unchanged for the Stokes photon $\omega_{s'}$ and results are now shown in Fig. 3. Unlike in the previous case Stokes absorption now exhibits the typical electromagnetically induced transparency narrow dip whose width $\delta_{EIT} \sim \Omega_c^2/\gamma_{32}$ gives approximately the linewidth of the entangled state. At double-photon resonance the absorption reaches a minimum of approximately 8‰ and such a small absorption affects also the mismatch $\delta_A^{(L)}$ that shows a peak exactly at the double-photon resonance (see Fig. 3(b)). The mismatch is otherwise bound to the background value of about 0.6, as the absorption of the coupling and driving fields remain strong. The (dimensionless)

Optics EXPRESS

nonlinear susceptibility $\chi_A^{(3)}$ in Fig. 3(c), again a purely imaginary function, is maximum at the double-photon resonance reaching values $2 \sim 3$ orders of magnitude larger than in the previous large-detuning case. At last, owing to the combined effect of the resonant enhancement of the nonlinearity and the very small absorption, both hinging on electromagnetically induced transparency with coupling and driving fields both resonant, $\mathcal{P}$ can reach values as high as 0.005 within a very narrow bandwidth (see Fig. 3(d)). Because both (nonlinear) mixing paths in Fig. 1(A,B) are "equally" enhanced, the generation of the state (18) can be attained with rather good efficiencies, here quantified in terms of the count rate per unit of pump intensity and bandwidth (*brightness*). The latter largely exceeds [61] the one obtained *e.g.* with a different yet simpler atomic level configuration [41], with both driving fields off resonance, but also the one obtained *e.g.* in [29], where only one resonant driving pump is used.

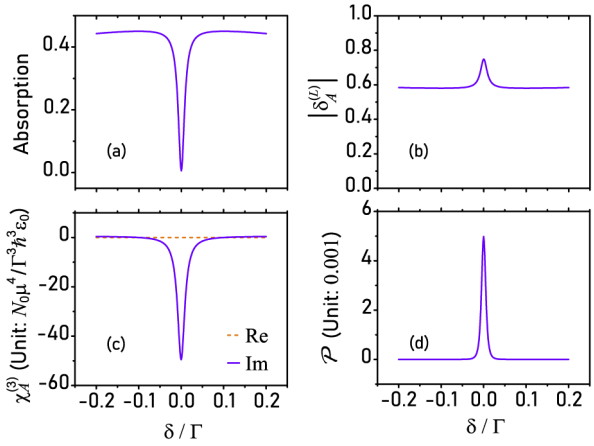

Fig. 3. *Resonant Color-Entanglement Generation*. Same as Fig. 2 but $\Delta_c = \Delta_{c'} = \Delta_d = 0$ and $\Omega_c = \Omega_{c'} = 0.05\,\Gamma$.

5. Entanglement engineering

In this last section we would like to investigate how to optimize the entanglement generation. Specifically, this amounts to identify regimes where large generation efficiencies ($\mathcal{P}$) occur with a concomitant high degree of entanglement. As a measurement of the entanglement we here adopt the negativity of the partial transpose (*NPT*), a concept based on the Peres-Horodecki separability criterion [62,63]. For our superposition state (18), we have

$$NPT = \frac{2}{\mathcal{P}} \times |f_A|\,|f_B| \tag{22}$$

taking on values ranging from 0 to 1 respectively for separable and maximally entangled states. Switching off, *e.g.* one of the coupling field ($f \to 0$) clearly makes $NPT \to 0$ while under conditions (10–11) and further assuming equal strengths of the applied couplings would make $NPT \to 1$, with $|\Psi\rangle_p$ being a maximally entangled in this case. As it may already be seen by inspection of Eqs. (14–15) and (18), the degree of entanglement basically relies on the relative strengths of the two coupling fields Ω_c and $\Omega_{c'}$ "provided" the two nonlinear susceptibilities for the spontaneous FWM processes have the same value and provided that mismatches are negligible. And it is instructive to notice that when Eqs. (10–11) and $\Omega_c = \Omega_{c'}$ both hold, it follows that $|\Psi\rangle_p \to |1_s, 0_{s'}\rangle + |0_s, 1_{s'}\rangle$, *i.e.* we attain a maximal entangled state, regardless of the values of the two-photon detuning δ.

Optics EXPRESS

We report in Fig. 4, the degree of entanglement (*NPT*) together with the generation efficiency ($\mathcal{P}$) for different values of Ω_c and $\Omega_{c'}$. We observe that maximal entanglement takes place over an appreciably wide region along the diagonal, while dropping quickly to zero as one unbalances the two coupling beam intensities. Notice that the maximal entanglement region is represented by a cone that widens for increasing coupling intensities and so does the efficiency that grows larger as $\mathcal{P} \propto |\Omega_c|^2 + |\Omega_{c'}|^2$. To this extent it's worth noting that we can not make $\mathcal{P}$ to increase at will so as to mantain the first-order perturbation expansion (13) valid.

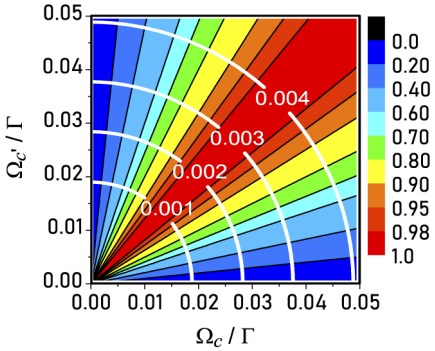

Fig. 4. Negativity of the partial transpose (*NPT*) (color scale) and generation efficiency ($\mathcal{P}$) (white lines) *vs.* the strength of the two coupling beams. Here $\Delta_c = \Delta_{c'} = \Delta_d = 0$, $\delta = 0$, $\Omega_d = 0.08\,\Gamma$. Other parameters are as in Fig. 2.

6. Conclusions

We have proposed an efficient scheme for heralded generation of single-photon narrowband color-entangled states in a cold atoms sample. Under certain circumstances, the selective excitation of two specific non-linear spontaneous four-wave mixing in a five-level configuration leads to the entanglement of two frequency modes (*color-entanglement*) being shared by a single Stokes photon. Weak losses and evenly balanced enhancement of these two nonlinear wave mixing processes lead to an improvement of the entanglement generation efficiency, as compared to apparently simpler generation schemes [41]. More generally, our results may also provide an advantage in improving [61] the generation efficiency of bi-photons with shaped temporal waveforms [31,32] where, unlike in the present work, a *single* four-wave mixing process underlays the generation of a Stokes-antiStokes pair. Besides weak losses and evenly balanced enhancement, both important experimental key factors in the generation of the state (18), the state's very narrow-bandwidth is another important feature, its relevance laying on the fact that (single-photon) line-widths smaller than the atomic line-width are essential *e.g.* in the storage of entanglement at distant locations (See *e.g.* [24]). Our proposal further allows for flexible manipulation of the degree of entanglement and optimization of its generation efficiency both of which may *e.g.* be enabled by a proper balance of the external driving fields parameters (see Figs. 2–4). The generation of maximally single-photon color-entangled states [10,46], as an example, can be attained under readily straightforward manipulation of the coupling fields driving conditions.

Appendix: the zero-order and first-order solutions

Let us consider the five-level system interacting with two coupling fields ω_c and $\omega_{c'}$ and a driving field ω_d, as shown in Fig. 1. Here ω_n, $n \in \{c, c', d\}$ stands for the frequency of the corresponding field. Under the law of energy and momentum, the Stokes photons ω_s, $\omega_{s'}$ and anti-Stokes

Optics EXPRESS

photons ω_{as} are spontaneously generated. For the convenience of the parameter choice, we take into account a specific ^{87}Rb atom for our five-level system, however this model can represent other media such as quantum dots or nitrogen-vacancy centers. In the rotating-wave approximations, the Hamiltonian describing the dynamics of such system is given by

$$\begin{aligned}\hat{H}/\hbar = &\delta\hat{\sigma}_{22} + \Delta_c\hat{\sigma}_{33} + \Delta_{c'}\hat{\sigma}_{44} + (\Delta_d + \delta)\hat{\sigma}_{55} - (\Omega_c\hat{\sigma}_{31} + \Omega_{c'}\hat{\sigma}_{41} + \Omega_d\hat{\sigma}_{52} + \text{H.c.}) \\ &- \frac{1}{2\hbar}(\mu_{15}\hat{E}^{+}_{as}\hat{\sigma}_{51} + \mu_{23}\hat{E}^{+}_{s}\hat{\sigma}_{32} + \mu_{24}\hat{E}^{+}_{s'}\hat{\sigma}_{42} + \text{H.c.}),\end{aligned} \tag{23}$$

with $\hat{\sigma}_{ij} = |i\rangle\langle j|$ $(i, j \in \{1, 2, 3, 4, 5\})$ serving as the atomic raising and lowering operators when $i \neq j$, and the atomic energy-level population operators when $i = j$ In Fig. 1, the double detuning δ is highlighted using the yellow color. The atom on the upper level $|j'\rangle, j' \in \{3, 4, 5\}$ decays through (optical) transition $|j'\rangle \leftrightarrow |j\rangle$ to the ground states $|j\rangle, j \in \{1, 2\}$ at the rate of $\Gamma_{jj'}$. The decoherence rate $\gamma_{jj'}$ of the transition is determined by the Lindbald operator $\mathcal{L}(\hat{\sigma}_{j'j})$ [46].

As discussed in the Sec. 2, the Heisenberg-Langevin equations of motion can be solved perturbatively. With $Q_{ij} = \sigma^{(0)}_{ii} - \sigma^{(0)}_{jj}$, the zero-order equations can be written as:

$$\frac{\partial\sigma^{(0)}_{55}}{\partial t} = -\sigma^{(0)}_{55}(\Gamma_{51} + \Gamma_{52}) - i\sigma^{(0)}_{25}\Omega^{*}_{d} + i\Omega_d\sigma^{(0)}_{52}, \tag{24a}$$

$$\frac{\partial\sigma^{(0)}_{44}}{\partial t} = -\sigma^{(0)}_{44}(\Gamma_{41} + \Gamma_{42}) - i\sigma^{(0)}_{14}\Omega^{*}_{c'} + i\Omega_{c'}\sigma^{(0)}_{41}, \tag{24b}$$

$$\frac{\partial\sigma^{(0)}_{33}}{\partial t} = -\sigma^{(0)}_{33}(\Gamma_{31} + \Gamma_{32}) - i\sigma^{(0)}_{13}\Omega^{*}_{c} + i\Omega_{c}\sigma^{(0)}_{31}, \tag{24c}$$

$$\begin{aligned}\frac{\partial\sigma^{(0)}_{22}}{\partial t} =&\Gamma_{32}\sigma^{(0)}_{33} + \Gamma_{52}\sigma^{(0)}_{55} + \Gamma_{42}\sigma^{(0)}_{44} \\ &+ i\sigma^{(0)}_{25}\Omega^{*}_{d} - i\Omega_d\sigma^{(0)}_{52},\end{aligned} \tag{24d}$$

$$\sigma^{(0)}_{11} + \sigma^{(0)}_{22} + \sigma^{(0)}_{33} + \sigma^{(0)}_{44} + \sigma^{(0)}_{55} = 1, \tag{24e}$$

$$\frac{\partial\sigma^{(0)}_{54}}{\partial t} = -g_{54}\sigma^{(0)}_{54} + i\Omega_{c'}\sigma^{(0)}_{51} - i\sigma^{(0)}_{24}\Omega^{*}_{d}, \tag{25a}$$

$$\frac{\partial\sigma^{(0)}_{34}}{\partial t} = -g_{34}\sigma^{(0)}_{34} + i\Omega_{c'}\sigma^{(0)}_{31} - i\sigma^{(0)}_{14}\Omega^{*}_{c}, \tag{25b}$$

$$\frac{\partial\sigma^{(0)}_{24}}{\partial t} = -g_{24}\sigma^{(0)}_{24} + i\Omega_{c'}\sigma^{(0)}_{21} - i\Omega_d\sigma^{(0)}_{54}, \tag{25c}$$

$$\frac{\partial\sigma^{(0)}_{14}}{\partial t} = -g_{14}\sigma^{(0)}_{14} - i\Omega_{c}\sigma^{(0)}_{34} + i\Omega_{c'}Q_{14}, \tag{25d}$$

$$\frac{\partial\sigma^{(0)}_{35}}{\partial t} = -g_{35}\sigma^{(0)}_{35} + i\Omega_d\sigma^{(0)}_{32} - i\sigma^{(0)}_{15}\Omega^{*}_{c}, \tag{25e}$$

$$\frac{\partial\sigma^{(0)}_{25}}{\partial t} = -g_{25}\sigma^{(0)}_{25} + i\Omega_d Q_{25}, \tag{25f}$$

$$\frac{\partial\sigma^{(0)}_{13}}{\partial t} = -g_{13}\sigma^{(0)}_{13} - i\Omega_{c'}\sigma^{(0)}_{43} + i\Omega_{c}Q_{13}, \tag{25g}$$

Optics EXPRESS

$$\frac{\partial\sigma_{12}^{(0)}}{\partial t} = -g_{12}\sigma_{12}^{(0)} - i(\Omega_c\sigma_{32}^{(0)} + \Omega_{c'}\sigma_{42}^{(0)} - \Omega_d^*\sigma_{15}^{(0)}), \tag{25h}$$

$$\frac{\partial\sigma_{23}^{(0)}}{\partial t} = -g_{23}\sigma_{23}^{(0)} + i\Omega_c\sigma_{21}^{(0)} - i\Omega_d\sigma_{53}^{(0)}, \tag{25i}$$

$$\frac{\partial\sigma_{15}^{(0)}}{\partial t} = -g_{15}\sigma_{15}^{(0)} + i(\Omega_d\sigma_{12}^{(0)} - \Omega_c\sigma_{35}^{(0)} - \Omega_{c'}\sigma_{45}^{(0)}), \tag{25j}$$

For the steady state, we can set $\partial\sigma_{ij}^{(0)}/\partial t = 0$, and find the solutions to the above equations, which are

$$\sigma_{34}^{(0)} = \frac{\Omega_{c'}\Omega_c^*(g_{14}Q_{13} + g_{13}^*Q_{14})}{g_{14}|\Omega_{c'}|^2 + g_{13}^*|\Omega_c|^2 + g_{14}g_{13}^*g_{34}}, \tag{26a}$$

$$\sigma_{14}^{(0)} = \frac{iQ_{14}\left(|\Omega_{c'}|^2 + g_{13}^*g_{34}\right)\Omega_{c'} - iQ_{13}|\Omega_c|^2\Omega_{c'}}{g_{14}|\Omega_{c'}|^2 + g_{13}^*|\Omega_c|^2 + g_{14}g_{13}^*g_{34}}, \tag{26b}$$

$$\sigma_{25}^{(0)} = \frac{iQ_{25}\Omega_d}{g_{25}}, \tag{26c}$$

$$\sigma_{13}^{(0)} = \frac{iQ_{13}(|\Omega_c|^2 + g_{14}^*g_{34}^*)\Omega_c - iQ_{14}\Omega_c|\Omega_{c'}|^2}{g_{13}|\Omega_c|^2 + g_{14}^*|\Omega_{c'}|^2 + g_{13}g_{14}^*g_{34}^*}, \tag{26d}$$

$$\sigma_{12}^{(0)} = \sigma_{54}^{(0)} = \sigma_{15}^{(0)} = \sigma_{23}^{(0)} = \sigma_{35}^{(0)} = \sigma_{24}^{(0)} = 0 \tag{26e}$$

The expressions for the Q_{ij}'s correspond to Eqs. (5) and (6). Then the susceptibilities for coupling field and the driving field can be obtained, and written as

$$\chi_c = \frac{\mathcal{N}|\mu_{13}|^2}{\epsilon_0\hbar}\frac{ig_{41}g_{43}Q_{13}}{g_{13}|\Omega_c|^2 + g_{41}|\Omega_{c'}|^2 + g_{41}g_{43}g_{13}} \tag{27a}$$

$$\chi_{c'} = \frac{\mathcal{N}|\mu_{14}|^2}{\epsilon_0\hbar}\frac{ig_{31}g_{34}Q_{14}}{g_{31}|\Omega_c|^2 + g_{14}|\Omega_{c'}|^2 + g_{31}g_{34}g_{14}} \tag{27b}$$

$$\chi_d = \frac{\mathcal{N}|\mu_{25}|^2}{\epsilon_0\hbar}\frac{iQ_{25}}{g_{25}} \tag{27c}$$

Note that in the case of the large detunings $\Delta_n \gg \Gamma_{j'j}$, or the small Rabi frequencies $\Omega_n \ll \Gamma_{j'j}$, $(n \in \{c, c', d\}, j' \in \{3, 4, 5\}, j \in \{1, 2\})$ which we discussed in Sec. II, χ_c and $\chi_{c'}$ can be further simplified as

$$\chi_c = \frac{\mathcal{N}|\mu_{13}|^2}{\epsilon_0\hbar}\frac{iQ_{13}}{g_{13}} \tag{28a}$$

$$\chi_{c'} = \frac{\mathcal{N}|\mu_{14}|^2}{\epsilon_0\hbar}\frac{iQ_{14}}{g_{14}} \tag{28b}$$

The first order equations are

$$\frac{\partial\sigma_{55}^{(1)}}{\partial t} = -i\left(\Omega_d^*\sigma_{25}^{(1)} - \Omega_d\sigma_{52}^{(1)} - i\sigma_{55}^{(1)}\Gamma_{51} - i\sigma_{55}^{(1)}\Gamma_{52} + E_{as}^-\sigma_{15}^{(0)}\mu_{15} - E_{as}^+\sigma_{51}^{(0)}\mu_{51}\right) \tag{29a}$$

$$\frac{\partial\sigma_{44}^{(1)}}{\partial t} = -i\left(\Omega_{c'}^*\sigma_{14}^{(1)} - \Omega_{c'}\sigma_{41}^{(1)} - i\sigma_{44}^{(1)}\Gamma_{41} - i\sigma_{44}^{(1)}\Gamma_{42} + E_{s'}^-\sigma_{24}^{(0)}\mu_{24} - E_{s'}^+\sigma_{42}^{(0)}\mu_{42}\right) \tag{29b}$$

$$\frac{\partial\sigma_{33}^{(1)}}{\partial t} = -i\left(\Omega_c^*\sigma_{13}^{(1)} - \Omega_c\sigma_{31}^{(1)} - i\sigma_{33}^{(1)}\Gamma_{31} - i\sigma_{33}^{(1)}\Gamma_{32} + E_s^-\sigma_{23}^{(0)}\mu_{23} - E_s^+\sigma_{32}^{(0)}\mu_{32}\right) \tag{29c}$$

Optics EXPRESS

$$\frac{\partial\sigma_{22}^{(1)}}{\partial t} = i\Omega_d^*\sigma_{25}^{(1)} - i\Omega_d\sigma_{52}^{(1)} + \sigma_{33}^{(1)}\Gamma_{32} + \sigma_{55}^{(1)}\Gamma_{52} + \sigma_{44}^{(1)}\Gamma_{42} + iE_s^-\sigma_{23}^{(0)}\mu_{23} + iE_{s'}^-\sigma_{24}^{(0)}\mu_{24} - iE_s^+\sigma_{32}^{(0)}\mu_{32} - iE_{s'}^+\sigma_{42}^{(0)}\mu_{42} \tag{29d}$$

$$\frac{\partial\sigma_{54}^{(1)}}{\partial t} = -i\left(\Omega_d^*\sigma_{24}^{(1)} - \Omega_{c'}\sigma_{51}^{(1)} - i\sigma_{54}^{(1)}g_{54} + E_{as}^-\sigma_{14}^{(0)}\mu_{15} - E_{s'}^+\sigma_{52}^{(0)}\mu_{42}\right) \tag{29e}$$

$$\frac{\partial\sigma_{34}^{(1)}}{\partial t} = -i\left(\Omega_c^*\sigma_{14}^{(1)} - \Omega_{c'}\sigma_{31}^{(1)} - i\sigma_{34}^{(1)}g_{34} + E_s^-\sigma_{24}^{(0)}\mu_{23} - E_{s'}^+\sigma_{32}^{(0)}\mu_{42}\right) \tag{29f}$$

$$\frac{\partial\sigma_{24}^{(1)}}{\partial t} = -i\left(-\Omega_{c'}\sigma_{21}^{(1)} + \Omega_d\sigma_{54}^{(1)} - i\sigma_{24}^{(1)}g_{24} + E_s^+\sigma_{34}^{(0)}\mu_{32} - E_{s'}^+\sigma_{22}^{(0)}\mu_{42} + E_{s'}^+\sigma_{44}^{(0)}\mu_{42}\right) \tag{29g}$$

$$\frac{\partial\sigma_{14}^{(1)}}{\partial t} = -i\left(\Omega_c\sigma_{34}^{(1)} + \Omega_{c'}\left(\sigma_{44}^{(1)} - \sigma_{11}^{(1)}\right) - i\sigma_{14}^{(1)}g_{14} + E_{as}^+\sigma_{54}^{(0)}\mu_{51} - E_{s'}^+\sigma_{12}^{(0)}\mu_{42}\right) \tag{29h}$$

$$\frac{\partial\sigma_{35}^{(1)}}{\partial t} = -i\left(\Omega_c^*\sigma_{15}^{(1)} - \Omega_d\sigma_{32}^{(1)} - i\sigma_{35}^{(1)}g_{35} + E_s^-\sigma_{25}^{(0)}\mu_{23} - E_{as}^+\sigma_{31}^{(0)}\mu_{51}\right) \tag{29i}$$

$$\frac{\partial\sigma_{25}^{(1)}}{\partial t} = i\left(\Omega_d\left(\sigma_{22}^{(1)} - \sigma_{55}^{(1)}\right) + i\sigma_{25}^{(1)}g_{25} - E_s^+\sigma_{35}^{(0)}\mu_{32} + E_{as}^+\sigma_{21}^{(0)}\mu_{51} - E_{s'}^+\sigma_{45}^{(0)}\mu_{42}\right) \tag{29j}$$

$$\frac{\partial\sigma_{15}^{(1)}}{\partial t} = i\left(\Omega_d\sigma_{12}^{(1)} - \Omega_c\sigma_{35}^{(1)} - \Omega_{c'}\sigma_{45}^{(1)} + i\sigma_{15}^{(1)}g_{15} + E_{as}^+\sigma_{11}^{(0)}\mu_{51} - E_{as}^+\sigma_{55}^{(0)}\mu_{51}\right) \tag{29k}$$

$$\frac{\partial\sigma_{23}^{(1)}}{\partial t} = i\left(\Omega_c\sigma_{21}^{(1)} - \Omega_d\sigma_{53}^{(1)} + i\sigma_{23}^{(1)}g_{23} + E_s^+\sigma_{22}^{(0)}\mu_{32} - E_s^+\sigma_{33}^{(0)}\mu_{32} - E_{s'}^+\sigma_{43}^{(0)}\mu_{42}\right) \tag{29l}$$

$$\frac{\partial\sigma_{13}^{(1)}}{\partial t} = -i\left(\Omega_c\left(\sigma_{33}^{(1)} - \sigma_{11}^{(1)}\right) + \Omega_{c'}\sigma_{43}^{(1)} - i\sigma_{13}^{(1)}g_{13} - E_s^+\sigma_{12}^{(0)}\mu_{32} + E_{as}^+\sigma_{53}^{(0)}\mu_{51}\right) \tag{29m}$$

$$\frac{\partial\sigma_{12}^{(1)}}{\partial t} = i\left(\Omega_d^*\sigma_{15}^{(1)} - \Omega_c\sigma_{32}^{(1)} - \Omega_{c'}\sigma_{42}^{(1)} + i\sigma_{12}^{(1)}g_{12} + E_s^-\sigma_{13}^{(0)}\mu_{23} + E_{s'}^-\sigma_{14}^{(0)}\mu_{24} - E_{as}^+\sigma_{52}^{(0)}\mu_{51}\right) \tag{29n}$$

Substituting the zeroth-order solution into the above equation, and solving the algebraic equation obtain from setting $\partial\sigma_{ij}^{(1)}/\partial t = 0$ will lead us to the solution given in Sec. 2. Note that for the resonant case with $\Omega_n \ll \Gamma_{j'j}$, or the large detuning case $\Delta_n \gg \Gamma_{j'j}$ ($n \in \{c, c', d\}, j \in \{1, 2\}$ and $j' \in \{3, 4, 5\}$), we only need to keep the terms up to second order with respect to coupling or driving Rabi frequencies (Ω_n) during the calculation. This is a very useful procedure and help us to get a relatively simpler but accurate enough expressions.

Funding

National Natural Science Foundation of China (11534002, 11674049, 11861131001); Cooperative Program by the Italian Ministry of Foreign Affairs and International Cooperation (PGR00960); "Laboratori Congiunti" 2019 Program of National Research Council of Italy.

Acknowledgments

The work is supported by the National Natural Science Foundation of China (No. 11534002 and No. 11674049), the Cooperative Program by the Italian Ministry of Foreign Affairs and International Cooperation (No. PGR00960) and the National Natural Science Foundation of China (No. 11861131001) and the "Laboratori Congiunti" 2019 Program of National Research Council of Italy.

Optics EXPRESS

Disclosures

The authors declare that there are no conflicts of interest related to this article.

References

1. A. I. Lvovsky and M. Raymer, "Continuous-variable optical quantum-state tomography," Rev. Mod. Phys. **81**(1), 299–332 (2009).
2. F. Flamini, N. Spagnolo, and F. Sciarrino, "Photonic quantum information processing: a review," Rep. Prog. Phys. **82**(1), 016001 (2019).
3. S. L. Braunstein and P. van Loock, "Narrowband biphoton generation in the group delay regime," Rev. Mod. Phys. **77**(2), 513–577 (2005).
4. R. Raussendorf and H. J. Briegel, "A one-way quantum computer," Phys. Rev. Lett. **86**(22), 5188–5191 (2001).
5. T. D. Ladd, F. Jelezko, R. Laflamme, Y. Nakamura, C. Monroe, and J. L. O'Brien, "Quantum computers," Nature (London) **464**(7285), 45–53 (2010).
6. A. Montanaro, "Quantum algorithms: an overview," npj Quantum Inf. **2**(1), 15023 (2016).
7. V. Giovannetti, "S. Lloyd, and L. Maccone," Phys. Rev. Lett. **96**(1), 010401 (2006).
8. J. L. O'Brien, A. Furusawa, and J. Vučković, "Photonic quantum technologies," Nat. Photonics **3**(12), 687–695 (2009).
9. M. D. Eisaman, A. M. J. Fan, and S. V. Polyakov, "Single-photon sources and detectors," Rev. Sci. Instrum. **82**(7), 071101 (2011).
10. U. Leonhardt, *Measuring the Quantum State of Light* (Cambridge University, 1997).
11. M. Artoni and R. Loudon, "Propagation of nonclassical light through an absorbing and dispersive slab," Phys. Rev. A **59**(3), 2279–2290 (1999).
12. M. Artoni and R. Loudon, "Quantum theory of optical-pulse propagation through an amplifying slab," Phys. Rev. A **57**(1), 622–628 (1998).
13. M. Artoni and J. L. Birman, "Non-classical states in solids and detection," Opt. Commun. **104**(4-6), 319–324 (1994).
14. H. J. Kimble, "The quantum internet," Nature (London) **453**(7198), 1023–1030 (2008).
15. B. M. Terhal, "Quantum error correction for quantum memories," Rev. Mod. Phys. **87**(2), 307–346 (2015).
16. V. Scarani, H. Bechmann-Pasquinucci, N. J. Cerf, M. Dušek, N. Lütkenhaus, and M. Peev, "The security of practical quantum key distribution," Rev. Mod. Phys. **81**(3), 1301–1350 (2009).
17. N. Gisin and R. Thew, "Quantum communication," Nat. Photonics **1**(3), 165–171 (2007).
18. P. G. Kwiat, K. Mattle, H. Weinfurter, A. Zeilinger, A. V. Sergienko, and Y. Shih, "New high-intensity source of polarization-entangled photon pairs," Phys. Rev. Lett. **75**(24), 4337–4341 (1995).
19. J. T. Barreiro, T.-C. Wei, and P. G. Kwiat, "Beating the channel capacity limit for linear photonic superdense coding," Nat. Phys. **4**(4), 282–286 (2008).
20. L. K. Shalm, D. R. Hamel, Z. Yan, C. Simon, K. J. Resch, and T. Jennewein, "Three-photon energy–time entanglement," Nat. Phys. **9**(1), 19–22 (2013).
21. X. L. Wang, L. K. Chen, W. Li, H. L. Huang, C. Liu, C. Chen, Y. H. Luo, Z. E. Su, D. Wu, Z. D. Li, H. Lu, Y. Hu, X. Jiang, C. Z. Peng, L. Li, N. L. Liu, Y. A. Chen, C. Y. Lu, and J. W. Pan, "Experimental ten-photon entanglement," Phys. Rev. Lett. **117**(21), 210502 (2016).
22. Z. Y. Zhou, S. L. Liu, Y. Li, D. S. Ding, W. Zhang, S. Shi, M. X. Dong, B. S. Shi, and G. C. Guo, "Orbital angular momentum-entanglement frequency transducer," Phys. Rev. Lett. **117**(10), 103601 (2016).
23. X. L. Wang, Y. H. Luo, H. L. Huang, M. C. Chen, Z. E. Su, C. Liu, C. Chen, W. Li, Y. Q. Fang, X. Jiang, J. Zhang, L. Li, N. L. Liu, C. Y. Lu, and J. W. Pan, "18-qubit entanglement with six photons' three degrees of freedom," Phys. Rev. Lett. **120**(26), 260502 (2018).
24. L. M. Duan, M. D. Lukin, J. I. Cirac, and P. Zoller, "Long-distance quantum communication with atomic ensembles and linear optics," Nature (London) **414**(6862), 413–418 (2001).
25. A. Kuzmich, W. P. Bowen, A. D. Boozer, A. Boca, C. W. Chou, L. M. Duan, and H. J. Kimble, "Generation of nonclassical photon pairs for scalable quantum communication with atomic ensembles," Nature (London) **423**(6941), 731–734 (2003).
26. S. Ritter, C. Nolleke, C. Hahn, A. Reiserer, A. Neuzner, M. Uphoff, M. Mucke, E. Figueroa, J. Bochmann, and G. Rempe, "An elementary quantum network of single atoms in optical cavities," Nature (London) **484**(7393), 195–200 (2012).
27. A. Stute, B. Casabone, B. Brandstatter, K. Friebe, T. E. Northup, and R. Blatt, "Quantum-state transfer from an ion to a photon," Nat. Photonics **7**(3), 219–222 (2013).
28. C. Shu, P. Chen, T. K. Chow, L. Zhu, Y. Xiao, M. M. Loy, and S. Du, "Subnatural-linewidth biphotons from a doppler-broadened hot atomic vapour cell," Nat. Commun. **7**(1), 12783 (2016).
29. V. Balic, D. A. Braje, P. Kolchin, G. Y. Yin, and S. E. Harris, "Generation of paired photons with controllable waveforms," Phys. Rev. Lett. **94**(18), 183601 (2005).
30. B. Srivathsan, G. K. Gulati, B. Chng, G. Maslennikov, D. Matsukevich, and C. Kurtsiefer, "Narrow band source of transform-limited photon pairs via four-wave mixing in a cold atomic ensemble," Phys. Rev. Lett. **111**(12), 123602 (2013).

Optics EXPRESS

31. J. F. Chen, S. Zhang, H. Yan, M. M. T. Loy, G. K. L. Wong, and S. Du, "Shaping biphoton temporal waveforms with modulated classical fields," Phys. Rev. Lett. **104**(18), 183604 (2010).
32. S. Du, J. Wen, and C. Belthangady, "Temporally shaping biphoton wave packets with periodically modulated driving fields," Phys. Rev. A **79**(4), 043811 (2009).
33. S. Du, J. Wen, M. H. Rubin, and G. Y. Yin, "Four-wave mixing and biphoton generation in a two-level system," Phys. Rev. Lett. **98**(5), 053601 (2007).
34. J. Wen, S. Du, and M. H. Rubin, "Biphoton generation in a two-level atomic ensemble," Phys. Rev. A **75**(3), 033809 (2007).
35. J. Wen, S. Du, and M. H. Rubin, "Spontaneous parametric down-conversion in a three-level system," Phys. Rev. A **76**(1), 013825 (2007).
36. S. Du, P. Kolchin, C. Belthangady, G. Y. Yin, and S. E. Harris, "Subnatural linewidth biphotons with controllable temporal length," Phys. Rev. Lett. **100**(18), 183603 (2008).
37. L. Zhao, Y. Su, and S. Du, "Narrowband biphoton generation in the group delay regime," Phys. Rev. A **93**(3), 033815 (2016).
38. H. Yan, S. Zhang, J. F. Chen, M. M. Loy, G. K. Wong, and S. Du, "Generation of narrow-band hyperentangled nondegenerate paired photons," Phys. Rev. Lett. **106**(3), 033601 (2011).
39. J. C. Lee, K. K. Park, T. M. Zhao, and Y. H. Kim, "Einstein-podolsky-rosen entanglement of narrow-band photons from cold atoms," Phys. Rev. Lett. **117**(25), 250501 (2016).
40. T. M. Zhao, Y. S. Ihn, and Y. H. Kim, "Direct generation of narrow-band hyperentangled photons," Phys. Rev. Lett. **122**(12), 123607 (2019).
41. A. Zavatta, M. Artoni, and G. La Rocca, "Engineering of heralded narrowband color-entangled states," Phys. Rev. A **99**(3), 031802 (2019).
42. D. Viscor, V. Ahufinger, J. Mompart, A. Zavatta, G. C. La Rocca, and M. Artoni, "Two-color quantum memory in double-λ media," Phys. Rev. A **86**(5), 053827 (2012).
43. Y. Niu, S. Gong, R. Li, Z. Xu, and X. Liang, "Giant kerr nonlinearity induced by interacting dark resonances," Opt. Lett. **30**(24), 3371–3373 (2005).
44. H. Schmidt and A. Imamoglu, "Giant kerr nonlinearities obtained by electromagnetically induced transparency," Opt. Lett. **21**(23), 1936–1938 (1996).
45. K. Hakuta, L. Marmet, and B. P. Stoicheff, "Electric-field-induced second-harmonic generation with reduced absorption in atomic hydrogen," Phys. Rev. Lett. **66**(5), 596–599 (1991).
46. M. O. Scully and M. S. Zubairy, *Quantum Optics* (Cambridge University, 1997).
47. M. Artoni, G. C. La Rocca, F. S. Cataliotti, and F. Bassani, "Highly anomalous group velocity of light in ultracold rubidium gases," Phys. Rev. A **63**(2), 023805 (2001).
48. M. Fleischhauer, A. Imamoglu, and J. P. Marangos, "Electromagnetically induced transparency: Optics in coherent media," Rev. Mod. Phys. **77**(2), 633–673 (2005).
49. Y.-W. Lin, W.-T. Liao, T. Peters, H.-C. Chou, J.-S. Wang, H.-W. Cho, P.-C. Kuan, and I. A. Yu, "Stationary light pulses in cold atomic media and without bragg gratings," Phys. Rev. Lett. **102**(21), 213601 (2009).
50. See e.g. D. A. Steck, "Rubidium 85 D line data, ru-bidium 87 D line data, cesium D line data," Technical Report (Los Alamos National Laboratory, 2008), available at http://steck.us/alkalidata.
51. M. Guo, H. Zhou, D. Wang, J. Gao, J. Zhang, and S. Zhu, "Experimental investigation of high-frequency-difference twin beams in hot cesium atoms," Phys. Rev. A **89**(3), 033813 (2014).
52. H. Cai, J. Liu, J. Wu, Y. He, S.-Y. Zhu, J.-X. Zhang, and D.-W. Wang, "Experimental observation of momentum-space chiral edge currents in room-temperature atoms," Phys. Rev. Lett. **122**(2), 023601 (2019).
53. Y. He, Y.-M. He, Y.-J. Wei, X. Jiang, K. Chen, C.-Y. Lu, J.-W. Pan, C. Schneider, M. Kamp, and S. Höfling, "Quantum state transfer from a single photon to a distant quantum-dot electron spin," Phys. Rev. Lett. **119**(6), 060501 (2017).
54. J. Klatzow, J. N. Becker, P. M. Ledingham, C. Weinzetl, K. T. Kaczmarek, D. J. Saunders, J. Nunn, I. A. Walmsley, R. Uzdin, and E. Poem, "Experimental demonstration of quantum effects in the operation of microscopic heat engines," Phys. Rev. Lett. **122**(11), 110601 (2019).
55. D. N. Klyshko, *Photons and Nonlinear Optics* (Gordon and Breach Science, 1988).
56. R. Loudon, *The Quantum Theory of Light* (Clarendon, 2000).
57. S. Du, J. Wen, and M. H. Rubin, "Narrowband biphoton generation near atomic resonance," J. Opt. Soc. Am. B **25**(12), C98–C108 (2008).
58. K. J. Blow, R. Loudon, S. J. D. Phoenix, and T. J. Shepherd, "Continuum fields in quantum optics," Phys. Rev. A **42**(7), 4102–4114 (1990).
59. M. Artoni and R. Loudon, "Quantum theory of optical pulse propagation through an absorbing and dispersive slab," Phys. Rev. A **55**(2), 1347–1357 (1997).
60. J.-H. Wu, M. Artoni, and G. C. La Rocca, "Parity-time-antisymmetric atomic lattices without gain," Phys. Rev. A **91**(3), 033811 (2015).
61. The count rate is given by $\int |f_{A,B}(\cdots)|^2 d\delta$ (See e.g. [29]). For the driving conditions and atomic parameters of Fig. 3(d) the brightness can be estimated as 5×10^5 pair count /(sec MHz mW/cm^2) and exceeds by more than one order of magnitude that obtained under equal conditions in [29], with 8×10^3 pair count /(sec MHz mW/cm^2), largely outdoing also well established large brightnesses as obtained *e.g.* in [36].
62. A. Peres, "Separability criterion for density matrices," Phys. Rev. Lett. **77**(8), 1413–1415 (1996).

Optics EXPRESS

63. M. Horodecki, P. Horodecki, and R. Horodecki, "Separability of mixed states: Necessary and sufficient conditions," Phys. Lett. A **223**(1-2), 1–8 (1996).